# Critical Layer Effects on Atmospheric Solitary and Cnoidal Waves

ERIC D. SKYLLINGSTAD

*Pacific Northwest Laboratory, Richland, Washington*

(Manuscript received 29 January 1990, in final form 18 December 1990)

ABSTRACT

The interactions of atmospheric cnoidal waves with a critical level are examined using a two-dimensional numerical model. A cnoidal wave system is generated by applying a bore initial condition to a shallow surface-based inversion; the system is analyzed using various profiles of stability and shear. Under neutral conditions a critical level is shown to cause wave reflection with wave growth, as indicated by the vertical velocity, when the stability is low. Increasing the ambient stability above the cnoidal wave leads to a reduction in the reflective properties of the critical level and an increase in critical level absorption. The division between wave growth and wave decay occurs near a critical level Richardson's number of 0.25 agreeing with instability theory. When a variable profile of stability is assumed, with stable regions both below and above the critical layer and weak stability at the critical level region, the cnoidal wave system again amplifies, but not as strongly. The results conform with past analytical results pertaining to the atmospheric structure required for wave reflection and absorption. However, the occurrence of overreflection cannot be diagnosed from the simulations because of the strongly nonlinear, unsteady behavior of the cnoidal wave systems.

## 1. Introduction

During the past decade, the subject of atmospheric solitary and cnoidal waves has received considerable attention in meteorological literature. These disturbances can result from the interaction of a strong surface front, such as a sea breeze or thunderstorm gust front, with a low-level inversion. The intrusion of cold, dense frontal air under the inversion leads to a jump condition in the inversion height known as a bore. Under proper atmospheric conditions, the bore will evolve into a series of internal waves, collectively referred to as cnoidal waves. After an extended period of time, the individual cnoidal wave components will separate to form "solitary" wave systems.

Cnoidal waves represent a potential trigger mechanism for early morning convective development. Intersections between pairs of thunderstorm outflow boundaries or gust fronts are known to be preferred regions for new convective initiation (Purdom 1976). When a strong surface inversion exists, cnoidal waves can replace the gust front in providing a surface disturbance. Cnoidal waves are well suited for this role since, unlike limited outflow regions that have strong frictional effects and inertial spreading, they propagate by a horizontally nondispersive oscillation of the stable boundary layer.

Observations of atmospheric cnoidal waves have identified both waves of depression (Pecnick and Young 1984; Bosart and Sanders 1986; Lin and Goff 1988) and waves of elevation (Christie et al. 1978; Doviak and Ge 1984; Haase and Smith 1984). Cnoidal waves of depression usually extend through the entire troposphere and appear as a trough of low pressure at the surface, whereas cnoidal waves of elevation are typically found on shallow inversions and cause a high-pressure spike at the surface.

Cnoidal gravity waves are known as waves of "permanent" form or weakly nonlinear waves. They exhibit steady-state form because of a balance between nonlinear and dispersive components in the equations of motion. In contrast, nonhydrostatic linear gravity waves are characterized by a strong dependence between the phase speed and the wavelength of the disturbance; they tend to disperse rapidly with time. Fundamental scales that discriminate between linear and nonlinear gravity waves are the depth of the propagation medium and the amplitude of the wave. With linear, internal gravity waves, the depth of the fluid is much greater than the wave amplitude, whereas with cnoidal waves, the waveguide or inversion depth is comparable to the wave amplitude.

Cnoidal waves propagate horizontally with little energy loss from wave dispersion when the overlying atmosphere is neutrally stratified. However, the actual atmosphere rarely exhibits a neutral stability profile but instead has various layers of stratification. Under these conditions, cnoidal waves lose energy through the vertical dispersion of internal, linear gravity wave modes. In order for cnoidal waves to exist without dissipation from gravity wave dispersion, a trapping mechanism must prevent vertically propagating modes.

*Corresponding author address:* Dr. E. Skyllingstad, Battelle, Pacific Northwest Laboratory, P.O. Box 999, Richland, WA 99352.

Previous modeling experiments of atmosphere cnoidal waves have considered either neutral atmospheric conditions (Christie 1989; Crook 1986) or situations with opposing shear and/or variable stratification (Crook 1988). Crook (1988) presents various examples of atmospheric profiles that will trap a cnoidal wave system with only marginal energy loss. In each case, the wave system is maintained by a reflection of energy from a change in stability and shear above the cnoidal wave. A trapping mechanism not considered in past efforts concerns the reflection of cnoidal waves by a critical level, which is the level where the wave phase velocity equals the ambient flow velocity. At this height, the internal wave interacts with the ambient flow, usually resulting in wave absorption. However, under weak stability conditions, a critical level can force wave reflection or overreflection and wave instability.

In this study, the interactions of cnoidal waves with a critical layer are examined using a two-dimensional nonhydrostatic numerical model. First, a short review on critical levels is presented, followed by a description of the numerical model and initial conditions. The main portion of the paper concerns the application of the model to the problem of cnoidal wave–critical layer interaction. Cnoidal waves are generated by initializing a bore on a surface inversion using a phase speed derived from solitary wave theory. Examples of weakening, neutral, and strengthening cnoidal wave systems are presented and contrasted to cases without a critical level.

## 2. Theory

When the atmosphere is statically stable, it is possible for internal vertically propagating gravity waves to exist. Almost any perturbation of a statically stable fluid will lead to internal gravity waves. The linear behavior of internal gravity waves can be described using the equation (Scorer 1949)

$$\frac{d^2\hat{w}}{dz^2} + m^2(z)\hat{w} = 0 \tag{1}$$

where

$$m^2(z) = l^2(z) - k^2$$

$$l^2(z) = \frac{N^2(z)}{(U-c)^2} - \frac{U_{zz}}{(U-c)}$$

$$N^2(z) = gd\ln\theta/dz$$

$$U_{zz} = \frac{\partial^2 U}{\partial z^2},$$

and $\hat{w}$ is a Fourier component magnitude of vertical motion, $\theta$ is potential temperature, $U(z)$ is the mean wind speed at height $z$, $c$ is the wave phase speed, $g$ is gravity, and $k$ is the horizontal wavenumber. The $l^2(z)$ term, commonly referred to as the Scorer parameter, is a measure of the propagation characteristics of the atmosphere in question. If a linear internal wave has a horizontal wavenumber, $k$, greater than $l(z)$, the wave cannot propagate through the fluid and is instead trapped below the region of small $l(z)$. A decrease in $l(z)$ and subsequent trapping can result from a reduction of $N$, large curvature of the wind profile ($U_{zz} < 0$), or an increase in the ambient wind relative to the wave speed (also known as Doppler ducting, see Chimonas and Hines 1986).

Trapping of gravity waves also occurs when the ambient flow $U$ equals the wave phase speed $c$. The level where $U = c$ is commonly referred to as the wave critical level because of the discontinuity in (1). Although solutions to (1) cannot be described at the critical level, the problem is still tractable near the region of criticality, with some imposed constraints. A thorough discussion of atmospheric critical levels is presented by Bretherton (1966) and Booker and Bretherton (1967) for cases where the gradient Richardson number

$$\mathrm{Ri} = N^2(z) \Big/ \left(\frac{\partial U}{\partial z}\right)^2 \tag{2}$$

exceeds the value of 0.25. Results from these papers indicate that the critical level can act as an absorber, with wave energy transferred to the mean flow.

The absorption can be quantified by examining the change in the horizontally averaged Reynold's stress

$$D(z) = \rho(z) \int [u'(x, z)w'(x, z)]dx \tag{3}$$

where

$$u'(x, z) = u(x, z) - U(z)$$

$$w'(x, z) = w(x, z) - W(z)$$

with $U(z)$ and $W(z)$ equal to the mean horizontal and vertical wind speeds. In an atmosphere with constant stability and wind speed, the Reynold's stress remains constant unless a critical level exists or nonlinear effects are dominant (Eliassen and Palm 1960). Changes in the vertical Reynold's stress profile indicate either wave absorption or wave reflection. Booker and Bretherton (1967) showed for a critical layer with Ri greater than 0.25 that the Reynold's stress of a linear gravity wave would decrease by a factor

$$\exp[-2\pi(\mathrm{Ri} - 0.25)^{1/2}] \tag{4}$$

as the wave propagated through the critical zone. If Ri in the vicinity of a critical level is less than approximately 0.25, a different solution exists for (1). As discussed by Jones (1968), linear gravity waves near a critical level with Ri less than 0.25 behave in a manner opposite to the solution of Booker and Bretherton, with

wave systems gaining energy at the expense of the mean flow instead of being absorbed. Following Jones, Lindzen and Tung (1978) demonstrated various conditions whereby a critical level can either partially reflect or overreflect incident linear wave systems. In addition to the mandatory condition of Ri less than 0.25, Lindzen and Tung suggested four additional conditions for a critical layer to overreflect:

1) a region must exist below the critical level with propagating wave solutions;
2) the critical level must be separated from the lower region by a trapping or evanescent layer;
3) a second region must exist above the critical level with propagating wave solutions;
4) a reflective surface must exist above the second region.

A later paper by Lindzen and Barker (1985) eliminated conditions 2 and 4 as essential preconditions. However, removal of the trapping layer (condition 2) is rarely achieved because of the requirement that Ri be less than 0.25 at the critical level.

Testing the importance of the overreflection criteria listed above is a principal task of this study. However, more important nonlinear processes that are not accounted for in overreflection theory may force gravity wave instability at a critical level. Therefore, the nonlinear simulations presented here must be carefully interpreted in view of the linearly derived overreflection requirements.

## 3. Numerical model and initial conditions

The numerical model used in this study is a derivative of the Klemp and Wilhelmson (1978) model as formulated by Cotton and Tripoli (1978). The model is based on the two-dimensional, fully compressible, nonhydrostatic, primitive equations with Fickian diffusion. The Fickian diffusion is added to control numerical nonlinear instabilities with the coefficients set to

$$K_x = 20 \text{ m}^2 \text{ s}^{-1}$$

$$K_z = 10 \text{ m}^2 \text{ s}^{-1}.$$

The model equations are solved using the popular time-splitting technique pioneered by Klemp and Wilhelmson (1978). Finite differencing is centered in time, centered in space on the long time step and forward in time, centered in space on the short time step, except for potential temperature, where a positive definite scheme by Smolarkiewicz (1983) is used. To further increase the model efficiency, the altered speed of sound approach or pseudocompressibility method used by Anderson et al. (1985) is employed with the speed of sound reduced to 150 m $s^{-1}$, decreasing the number of short model time steps by a factor of 2. All time differencing is performed explicitly without a semi-implicit vertical term (see Klemp and Wilhelmson 1978).

The domain extends 64 km in the horizontal by 10.5 km in the vertical with grid spacing of 250 m and 70 m, respectively, giving short and long time steps of 0.25 and 2.0 s. The two-dimensional framework and grid spacing were selected to match both the observational and analytical characteristics of undular bores and solitary waves. Boundary conditions for the model are radiative at both the top and sides. The top boundary condition is prescribed using the method suggested by Klemp and Durran (1983), which allows vertical gravity wave modes to propagate energy out of the model. At the lateral boundaries, the modified Sommerfield radiation condition proposed by Orlanski (1976) is applied. This method calculates the mean linear gravity wave phase speed and transports model state variables out of the model when an outflow condition occurs. At the bottom boundary a simple free-slip condition is imposed. A more formal discussion of the model is presented by Skyllingstad (1986).

The model initial conditions are prescribed using the vertical potential temperature function

$$\theta(z) = \theta(0)\left[1 + \frac{N^2(0)h}{g}\tanh(z/h)\right] \quad (5)$$

where $z$ is streamline height, $\theta(0)$ and $N^2(0)$ are the potential temperature and Brunt–Väisälä frequency at the surface, and $h$ is the inversion depth. This temperature structure was used by Grimshaw (1981) for an analytical calculation of solitary waves. Based on Grimshaw's results, a solitary wave phase speed, $c$, can be calculated using

$$c = \left[\frac{N^2(0)h^2}{2}\left(1 + \frac{3a}{5h}\right)\right]^{1/2} \quad (6)$$

where $a$ is the wave amplitude. Grimshaw's solution is used in the current simulations as an estimate of the cnoidal wave speed for the initial model inflow.

The equation defining the bore is

$$z = z_{\text{grid}} - \frac{1}{2}d\left[1 + \tanh\left(\frac{2}{5}x\right)\right] \quad (7)$$

where $z$ is the unperturbed height of the streamline that should pass through the gridpoint, $z_{\text{grid}}$ is the known height of the grid point, and $d$ is the vertical displacement defining the bore. The phase speed of a solitary wave with an amplitude equal to the bore displacement is assumed for the uniform flow and streamfunction calculation. This scaling is chosen so that bore-excited waves will, to a first approximation (some adjustment is necessary), remain stationary within the model domain. By multiplying the solution height by the solitary wave phase speed $c$, from (6), the streamfunction at the grid point, $\psi(x, z) = cz$, is determined. Horizontal and vertical velocity are calculated with

$$u = \frac{\partial \psi}{\partial z}$$

$$w = -\frac{\partial \psi}{\partial x}. \tag{8}$$

Vertical shear in the horizontal wind is prescribed by adding the vertical gradient after initializing the perturbation wind fields. The perturbation potential temperature is found by assuming potential temperature to be constant on streamlines (adiabatic flow) and substituting $z$ from (7) into (5). Finally, the initial perturbation pressure is computed from the perturbed potential temperature by assuming a hydrostatic balance.

To test the numerical model, solitary wave solutions from Grimshaw (1981) were initialized for solitary waves with amplitude 100, 300, and 600 m with a 600-m surface-inversion scale depth. The model was run for 48 simulation min and the results compared to the analytical solutions. The modeled phase speeds for the three cases were 12.28, 14.14, and 14.99 m $s^{-1}$, respectively, as compared to the analytical phase speeds of 11.57, 12.58, and 13.95 m $s^{-1}$. In addition to the phase speed differences, the numerical model solitary-wave wavelength slowly increases as a function of time. Differences between the two solutions are caused by the nonlinear nature of solitary waves as the amplitude is increased and inherent resolution problems are associated with the discrete model grid. The weakly nonlinear theory used to derive analytical solutions does not accurately describe solitary waves with large amplitude. As a consequence, for waves of high amplitude the model phase speeds are larger than the analytical predictions.

## 4. Results

In this section, four experiments are presented starting with a reference bore case (experiment 1), followed by three critical layer experiments. In the first critical layer experiment (experiment 2), cases are examined with different values of constant ambient stratification above the surface bore propagation inversion. The sensitivity of cnoidal waves to a critical level with different values of stratification is examined in these examples. Next, in experiment 3, simulations with vertically dependent stratification are presented to investigate the effects of trapping layers and relate the theories of overreflection discussed in section 2 to the numerical experiments. The results are concluded with an experiment to determine how cnoidal waves are influenced by ambient conditions that do not have a critical layer, but have shear in the same direction as the cnoidal wave motion (experiment 4). Situations of this type may be important during thunderstorm events because the relative speed of gust front propagation is often greater than the upper-level wind component in the direction of the gust front movement.

The bore initialization procedure defined in section 3 is used with the parameters

$$d = 600 \text{ m} \qquad h = 600 \text{ m}$$

$$\theta(0) = 290 \text{ K} \qquad N(0) = 0.026 \text{ s}^{-1}$$

for all simulations. The low-level (below approximately 2 km) momentum and temperature fields in each experiment are based on the initialization shown in Fig. 1, representing the reference bore case without ambient wind shear or upper level stratification. Upper-level stratification and shear in experiments 2, 3, and 4 are initialized by altering the model profiles so as to match those shown in Figs. 2a–c. Horizontal wind shear is set to $-5$ m $s^{-1}$ for each 1000 m with a minimum horizontal wind speed of $-10$ m $s^{-1}$ as presented in Fig. 2c. An exception is experiment 4 where the sensitivity

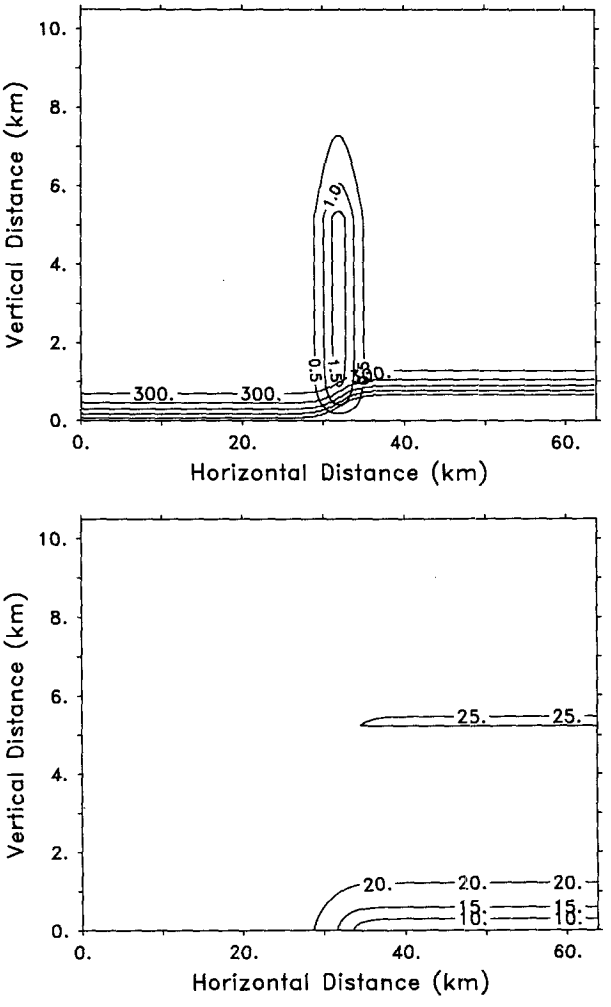


FIG. 1. Reference bore initial conditions of potential temperature (contour interval 2 K) and vertical velocity (contour interval 0.5 m $s^{-1}$) in (a) and horizontal velocity (contour interval 5 m $s^{-1}$) in (b). This initial state is used in each bore simulation with changes in the overlying shear and stratification specified as in Fig. 2.

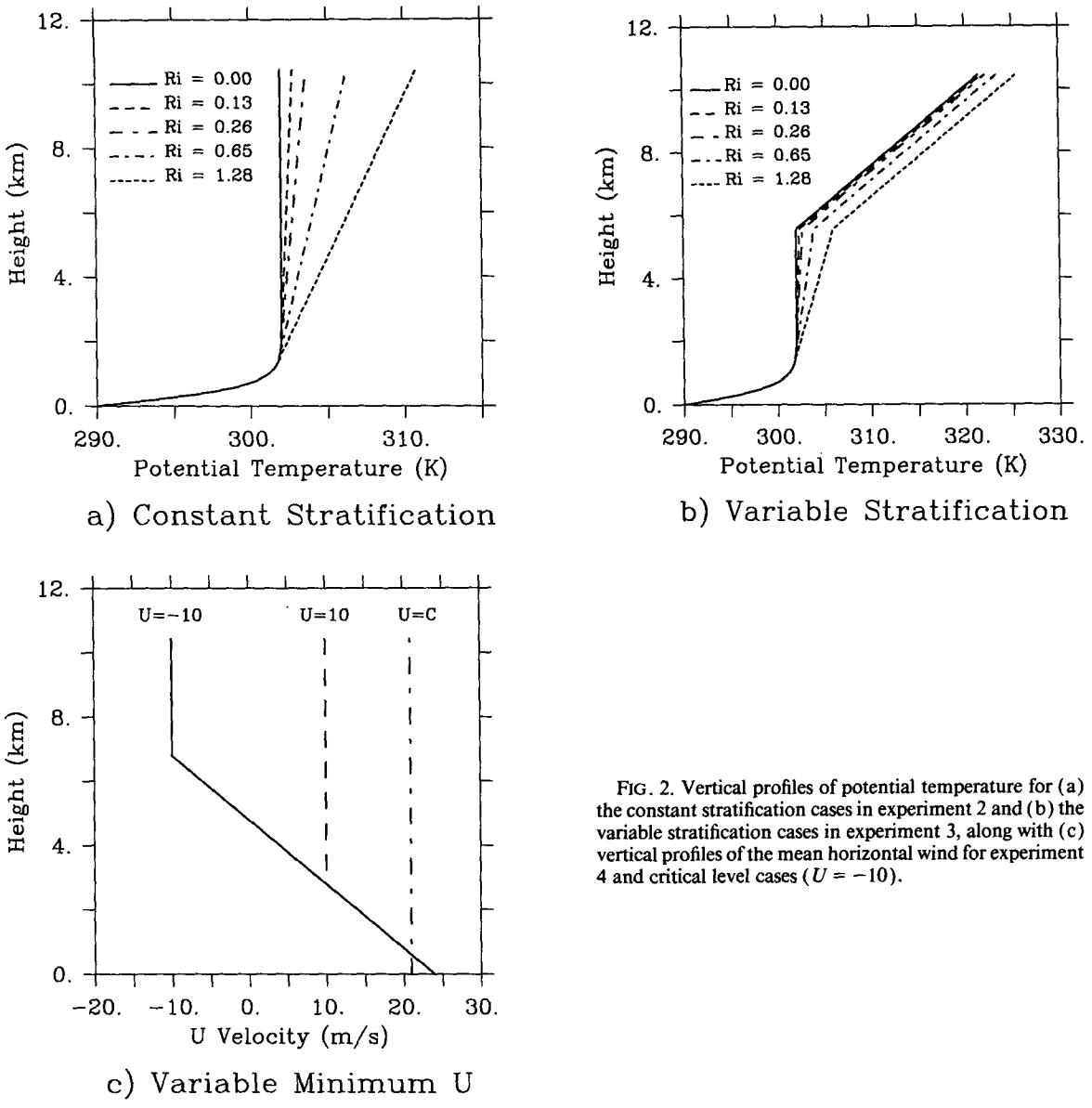


FIG. 2. Vertical profiles of potential temperature for (a) the constant stratification cases in experiment 2 and (b) the variable stratification cases in experiment 3, along with (c) vertical profiles of the mean horizontal wind for experiment 4 and critical level cases ($U = -10$).

to shear depth is examined by changing the minimum horizontal velocity. The profile labeled $U = -10$ in Fig. 2c represents the horizontal winds in experiments 2 and 3. To maintain stationary cnoidal waves, the base inflow velocity must be increased from the reference bore case by 2 to 4 m $s^{-1}$ in most of the cases to counter the effects of decreased upper-level winds and subsequent changes in the cnoidal wave phase speed. With this initialization, the critical level height is defined as the level where $U = 0$ or near 4.8 km in Fig. 2c.

### *a. Experiment 1: Reference bore case*

The first simulation represents a reference bore–cnoidal wave that will be used for comparison to critical layer simulations. A plot of the potential temperature, vertical velocity, and horizontal wind speed is shown in Figs. 3a,b after 96 min of simulated time. The production of cnoidal waves follows the classic bore problem (Crook 1986; Christie 1989) with the formation of an asymmetric bore front gradually leading to a train of slower moving cnoidal waves of smaller amplitude. In this example, only the first two cnoidal wave components are produced within the simulation period. The surface conditions exhibit a strong pressure increase and wind gust, but without a significant change in temperature as is typically noted with gust fronts. Only a small amplitude internal wave at the model top transports wave energy out of the model domain. As a result, the growth of the cnoidal wave progresses without significant loss of amplitude or wave energy.

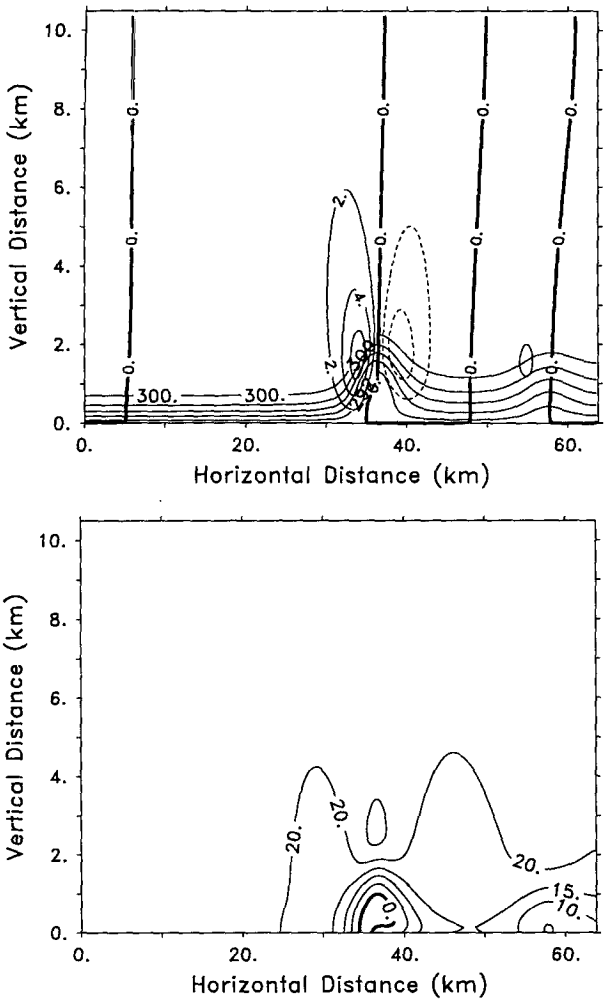


FIG. 3. Results from experiment 1 at 96 min showing (a) potential temperature (contour interval 2 K) and vertical motion (contour interval 2 m $s^{-1}$) and (b) horizontal motion (contour interval 5 m $s^{-1}$).

This follows the behavior described by (1) when $l(z)$ drops rapidly with height.

The structure of the leading cnoidal wave in Fig. 3a is of interest in comparison to the classic solitary wave. When the ratio $a/h$ approaches O(1) a solitary wave begins to increase in width and can eventually develop a recirculation in the wave center. In the current case, the wave is much wider than the weakly nonlinear theory of Benjamin (1967) predicts, with weak recirculation indicated by the negative horizontal velocity at the wave center. The phase speed for this case, 19.7 m $s^{-1}$, is relatively close to the predicted theoretical value of 17.78 m $s^{-1}$ using (6) with $a = 1600$ m and $h = 600$ m. Phase speed differences can be attributed to the small amplitude assumption ($a/h \ll 1$) used in the weakly nonlinear theory. The trailing cnoidal wave phase speed is less than the leading wave by approximately 2 m $s^{-1}$ because of the lower wave amplitude, as qualitatively predicted by (6). Many other general features noted with the classic solitary wave occur with the leading cnoidal wave, namely, almost symmetric vertical motion and potential temperature fields and a solitary surface wind gust with each wave component.

### *b. Experiment 2: Critical layer, constant stratification*

In experiment 2, results are presented for cases with uniform upper-level stratification (Fig. 2a) and constant shear profiles with a critical level near 4.8 km height (Fig. 2c, $U = -10$). First, cnoidal wave results for neutral conditions (Ri = 0) are discussed, followed by a case with stronger upper-level stability (Ri = 1.28). Plots of the potential temperature and vertical velocity for the Ri = 0 case are shown in Fig. 4. Vertically, the cnoidal wave system is similar to the reference bore case up to about 2 km. At that height the cnoidal wave vertical motion decays at a greater rate than the reference bore example. The rapid decrease in $w$ with this case can be examined by considering (1) in the vicinity of the critical level. If we assume constant shear and stratification, then (1) can be written as

$$\frac{d^2w}{dz^2} + \left[\frac{\mathrm{Ri}}{z^2} - k^2\right]w = 0 \qquad (9)$$

where the height of the critical level is set to 0. If we take $k = 0$, then a solution to (9) can be found for Ri less than 0.25:

$$w(z) \sim z^{1/2} \exp[\pm(0.25 - \mathrm{Ri})^{1/2} \ln z] \qquad (10)$$

as presented by Lindzen et al. (1980). This result implies that an exponential decrease in $w$ will occur near a critical level when the Ri is less than 0.25, even though $m(z)$ is greater than 0. The current example tends to-

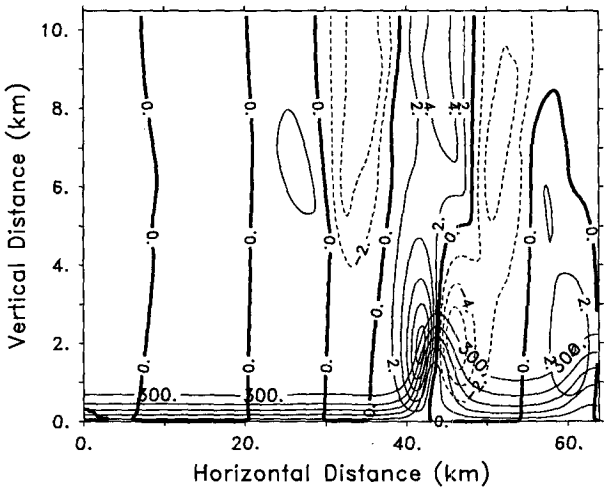


FIG. 4. Results from experiment 2 with Ri = 0.0 showing the vertical motion and potential temperature at 96 min. Contour intervals are the same as Fig. 3a.

ward this behavior with $w$ decreasing rapidly from a maximum of about 10 m s$^{-1}$ at the top of the bore, to about 2 m s$^{-1}$ at the critical level. Above the critical level, the vertical motion field shows a series of wave features of wavelength near 20 km. These disturbances are generated by the interaction of the cnoidal wave with the critical level and resemble large scale turbulent eddies. The wavelengths of these eddies are too small, when compared to the Scorer parameter wavelength, to be gravity wave modes and will, therefore, not be discussed further. In addition, the eddies are only generated in the Ri = 0.0 case, which is rarely observed in the atmosphere at the modeled heights.

The next case represents a stratified upper atmosphere with results shown in Fig. 5 at 48 min. Clearly, the critical level absorption process described by Booker and Bretherton (1967) is active with rapid decay of the cnoidal wave system when compared to the neutral case. If we assume that nonlinear effects are small outside of the critical region, then the attenuation of Reynold's stress with this case should be nearly 100% as the wave propagates through the critical layer [see Eq. (4)]. A plot of the simulated Reynold's stress from (3) as a function of time and height is presented in Fig. 6 with $U(z)$ and $W(z)$ defined as

$$\bar{U}(z(j)) = \frac{1}{256}\sum_{i=1}^{256} u(x(i), z(j))$$

$$\bar{W}(z(j)) = \frac{1}{256}\sum_{i=1}^{256} w(x(i), z(j)) \qquad (11)$$

where $i$ is the horizontal grid index extending from 1 to 256, and $j$ is the vertical grid index extending from 1 to 150. This plot shows a strong decrease in the Reynold's stress with height at the critical layer (about

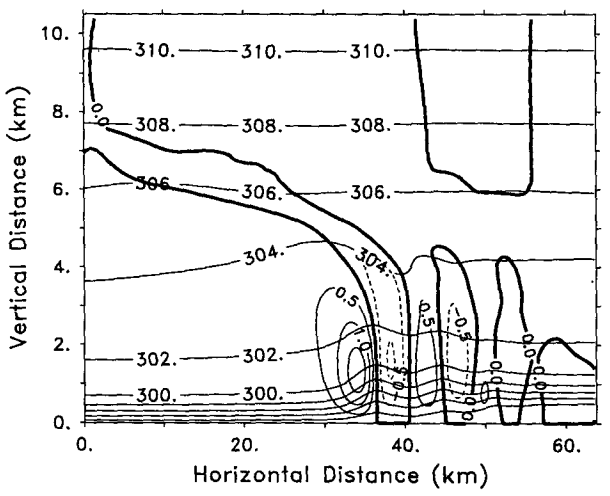


FIG. 5. Results from experiment 2 with Ri = 1.28 at 48 min. Variables and contour intervals are the same as Fig. 3a except for the contour interval of vertical motion, which is 0.5 m s$^{-1}$.

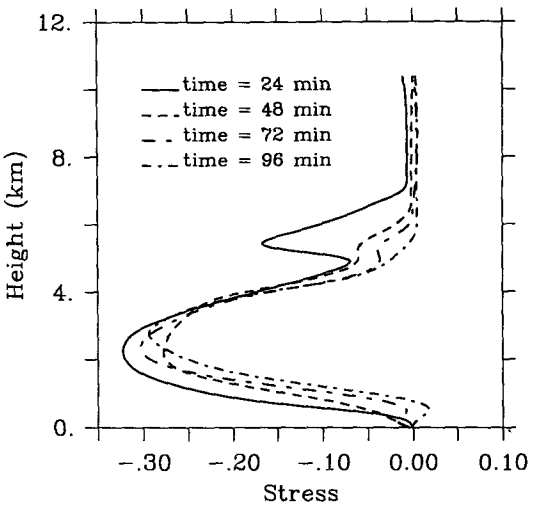


FIG. 6. Reynold's stress as a function of height at 24, 48, 72, and 96 min for the experiment 2 case with Ri = 1.28.

5 km), agreeing with (4). Also noticeable is a region of small scale turbulentlike motions at the critical level as indicated by the secondary minimum in Reynold's stress at 5.6 km. The secondary minimum decays with time as the wave amplitude approaches a steady state.

In Bretherton's conceptual model of critical level absorption, the wave packet has an asymptotically decreasing vertical wavelength as it approaches the critical level. The modeled wave system in Fig. 5 shows short horizontal wavelengths (10 km) and an exaggerated forward tilt near the critical level at about 5 km corresponding to the Reynold's stress minimum discussed above. However, the scale of motion does not contract to the grid resolution, which would be expected in the linear model. This does not mean that the current results are incorrect. The model critical level absorbs wave energy without requiring strong turbulent diffusion or increasingly smaller scale motions. The smallest scale shown in the model is much greater than the minimum resolvable scale, indicating that wave energy is transferred directly to the background or mean state. More evidence for this effect is found by calculating the terms defining the time rate of change of mean horizontal momentum (see Schlesinger 1990) at 48 min using the averaging method from (11). In the vicinity of the critical level, these terms are

$$\underset{-0.000231}{\frac{\partial \bar{U}}{\partial t}} + \underset{0.000054}{\overline{U\frac{\partial U}{\partial x}}} + \underset{-0.000398}{\overline{W\frac{\partial U}{\partial z}}} + \underset{0.000413}{\overline{\frac{1}{\rho}\frac{\partial P}{\partial x}}} - \underset{-0.000014}{K_x\frac{\partial^2 \bar{U}}{\partial z}} = \underset{-0.000202}{-\frac{\partial \overline{u'w'}}{\partial z}}$$

where overbars represent horizontal averages, showing a nonlinear transfer of wave momentum into the mean

pressure gradient and horizontal momentum gradients with Fickian diffusion having a small influence. These terms are calculated as horizontal averages and, therefore, do not sum to exactly zero because of finite differencing inconsistencies, implicit numerical diffusion, and problems in determining a mean wind field. However the residual, 0.000026 m $s^{-2}$, is an order of magnitude smaller than the key individual terms.

The uniform stratification experiments are concluded with a comparison of the maximum vertical motion for five different stratification values from Fig. 2a as shown in Fig. 7. The cases presented in Figs. 4 and 5 are labeled with Ri = 0.0 and Ri = 1.28, respectively. Two points are of interest with regard to Fig. 7. First, the maximum vertical motion shows an increase for all cases with Ri less than about 0.65. In each case, the initial growth of the leading cnoidal wave occurs because of the collapse of the bore. When Ri = 0.65, the leading cnoidal wave loses energy through absorption at the critical level as fast as it is produced from the bore collapse and partial wave reflection. The three processes of critical level absorption, critical level reflection, and bore collapse act together to produce the steady vertical velocity in this case. To help separate wave growth related to bore collapse from critical layer related amplification, we compare the test cases to the reference bore case shown in Fig. 3 and labeled "Reference" in Fig. 7. Waves that have a vertical velocity growth rate that is higher than the neutral, unsheared cnoidal wave case (Fig. 3) are considered unstable. Using this definition, the constant stratification cases are unstable and amplifying if Ri is greater than about 0.25.

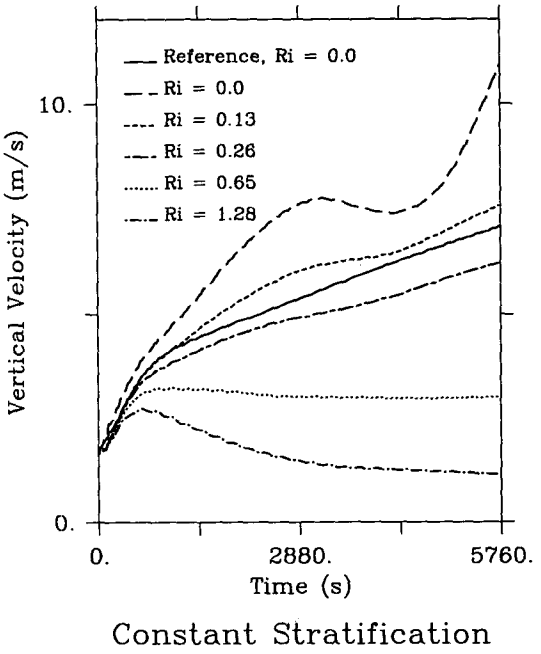


FIG. 7. Maximum vertical motion as a function of time for the reference bore and the five constant stratification cases from experiment 2.

The second point concerns the variable vertical motion growth rate for the neutrally stable case labeled Ri = 0. Animation of the results from this case demonstrates that the initialized bore cnoidal wave rapidly steepens, leading to a maximum in vertical motion at 48 min. Afterwards, a second cnoidal wave forms and the leading wave broadens slightly, resulting in a lower maximum vertical motion. The linkage between the formation of the secondary cnoidal wave and the reduction in wave growth is related to the horizontal dispersion characteristics of the cnoidal waves. In the stratified cases, secondary wave formation is more rapid and leads to a well-defined train of cnoidal waves (i.e., Fig. 5). Subsequently, the separation between the leading and secondary waves is reduced, limiting the growth of the lead wave. Also, as the stratification is increased, the wave systems behave more like linear waves because of the relative increase in the surface-based inversion depth in relation to the wave amplitude. Consequently, energy from the bore collapse is more uniformly distributed by horizontal wave dispersion in the stratified case.

The results presented here may conflict with the overreflection profile requirements discussed in section 2. In particular, the upper-level waveguide requirement (condition 3) does not seem to be an important condition for producing wave instability. As shown in Fig. 7, when the critical layer Ri is 0.13, the cnoidal wave shows increased amplitude when compared to the reference cnoidal wave. However, care must be used when applying these results to determine if overreflection is generating cnoidal wave growth. The cnoidal wave amplification is also dependent on reflected energy from the bore collapse. Although the process of overreflection cannot be separated from the other growth mechanisms, we can test if an upper-level stable region increases cnoidal wave reflection, supporting condition 3. This test is performed in the next experiment.

### c. *Experiment 3: Critical layer, variable stratification*

In this experiment, the upper-level stratification is altered from experiment 2 to examine the effects of two layers with differing stratification above the surface inversion. In these cases, the initialization is the same as the constant stratification simulations except for the potential temperature above 5600 m, which is set to a uniform value of 4 K/1000 m (Fig. 2b). The goal of this experiment is to simulate the effects of a wave propagation region above the critical layer, which may increase critical layer reflection as indicated in section 2 and lead to a stronger cnoidal wave amplification. Furthermore, the initial conditions in this experiment more closely resemble the actual atmospheric structure, when compared to the above constant-stratification cases.

The time history of the maximum vertical velocity for the six cases is shown in Fig. 8. Comparison of this plot with the uniform stratification examples in Fig. 7 shows that the presence of the upper-level propagation medium has a small influence on whether the leading wave system decays or grows. For example, the growth of maximum vertical motion for the Ri = 0.13 case is roughly the same as the uniform stratification example in Fig. 7. It is apparent from these two cases that the existence of an upper-level stable layer does not enhance wave growth. In fact, when Ri = 0 the increase in vertical velocity is less than the corresponding uniform stratification case. These results may indicate that the overreflection requirements listed in section 2 are not applicable in conditions of strong nonlinear motions and accompanying unsteady flow.

The wave amplification is more uniform in the current case when compared to the unsteady growth rate noted with experiment 1 for Ri = 0. The smooth wave growth is a result of the overlying stratified layer, which tends to force shorter wavelength cnoidal waves because of the more stable mean vertical structure. For instance, the average upper-level value of the Scorer parameter, $l(z)$, yields a minimum wavelength, $\lambda = 2\pi/l(z)$, of about 3 km in the variable stratification case, whereas with constant stratification the bounding wavelength is over 100 km.

### *d. Experiment 4: Variable shear*

In experiment 4, the vertical temperature profile is set to the experiment 3 cases with Ri = 0 and Ri = 0.65.

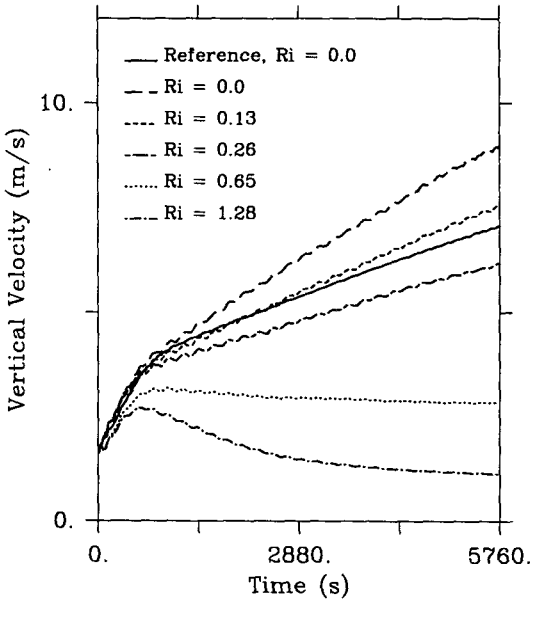


FIG. 8. Maximum vertical motion as a function of time for the reference bore case and the five variable stratification cases from experiment 3.

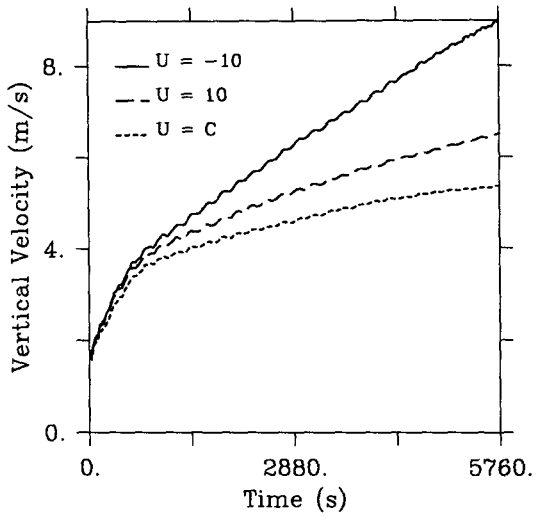


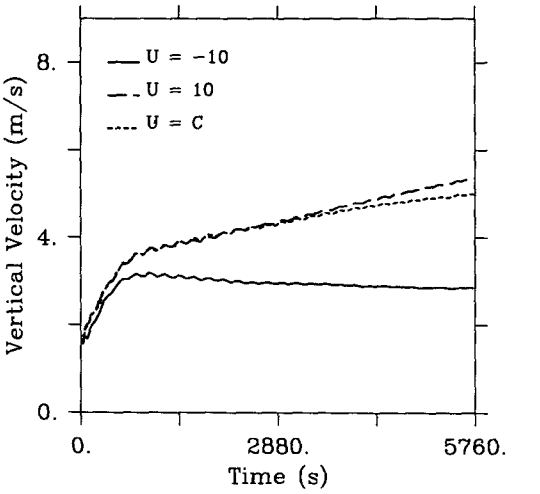


FIG. 9. Maximum vertical motion as a function of time for experiment 4 cases with (a) Ri = 0.0 and (b) Ri = 0.65. Profiles of the initialized ambient shear are shown in Fig. 2c for both cases.

The upper-level winds are varied from a minimum of −10 to a completely unsheared case, as shown in Fig. 2c. These wind shear configurations are meant to test the reflective properties of a layer that is near critical but does not have a complete wind direction reversal.

Results from the Ri = 0 cases are presented in Fig. 9a, showing a consistent increase in growth rate as the shear layer depth is expanded. In contrast, when Ri = 0.65, the growth rate decreases with increasing shear depth because the developing critical level begins to absorb a portion of the reflecting waves (Fig. 9b). When $U_{min} = 10$ and $U_{min} = c$ the growth rates are nearly identical, which can be explained by calculating $l(z)$. The changes in $l(z)$ from decreased $U$ do not strongly affect the midlevel wave propagation characteristics for

internal waves induced from the cnoidal waves. For example, when $U_{min} = 10$ the midlevel limiting wavelength is about 15 km, while the $U_{min} = c$ case gives a limiting wavelength of 32 km. Both of these values are near the cnoidal wavelength of between 10 and 20 km and allow partial wave propagation.

The case where $U_{min} = -10$ and Ri = 0.65 may help explain why thunderstorm outflow boundaries often dissipate rapidly during the evening hours. In most nocturnal thunderstorm cases, the upper-level stability is strong enough to produce critical layer absorption rather than reflection, assuming dry processes are dominant. The absorption of gravity wave energy by a critical level happens much more rapidly than the removal by internal wave propagation. As a result, critical levels hasten the decay of outflow boundaries, except when the upper-level stratification is weak.

As a last example, a plot of the potential temperature and vertical motion for the $U_{min} = c$ and $U_{min} = -10$ cases with Ri = 0 is presented in Figs. 10 and 11. In the unsheared case (Fig. 10), internal waves propagate away from the surface cnoidal system in both the vertical and horizontal directions, much like a classic mountain wave disturbance. These waves decrease the strengthening of the bore-induced waves by transporting energy out of the model domain. The critical level example (Fig. 11) shows a higher amplitude surface cnoidal wave and weaker transmitted internal waves in the upper stratified layer. Finally, with decreased winds aloft, the vertical wavelength in the upper layer is less than the unsheared case, concentrating the internal wave motion directly over the leading surface cnoidal wave.

## 5. Discussion and conclusions

If an actual atmospheric cnoidal wave existed with the characteristics presented in Fig. 11, it would likely evolve into a convective disturbance before developing wavelike structures. Many theories of squall line development employ gravity wave systems to explain convective line propagation (e.g., wave-CISK). Convective redevelopment and propagation could result from overreflecting cnoidal wave systems preceding squall line outflow, particularly at night with mesoscale convective complexes (MCC). A composite model of MCCs presented by Cotton et al. (1989) lends further evidence for critical level reflection of energy from the outflow preceding MCCs. Their analysis revealed a consistent motion of the MCCs in the same direction as a component of the flow aloft and indicated a moderate inversion at the surface during the mature and decay stages of the systems. The nocturnal surface inversion would provide the propagation medium for the cnoidal wave systems as portrayed in this paper.

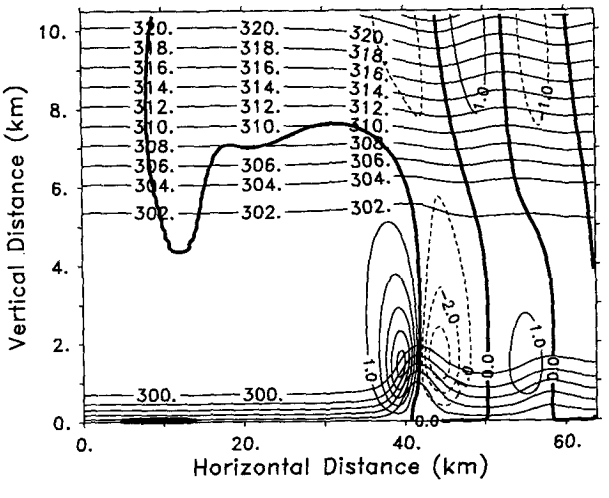


FIG. 10. Results from experiment 4 with Ri = 0.0 and $U_{min} = c$ (i.e., no shear). Contour intervals are the same as Fig. 3a except for vertical motion (1 m s$^{-1}$).

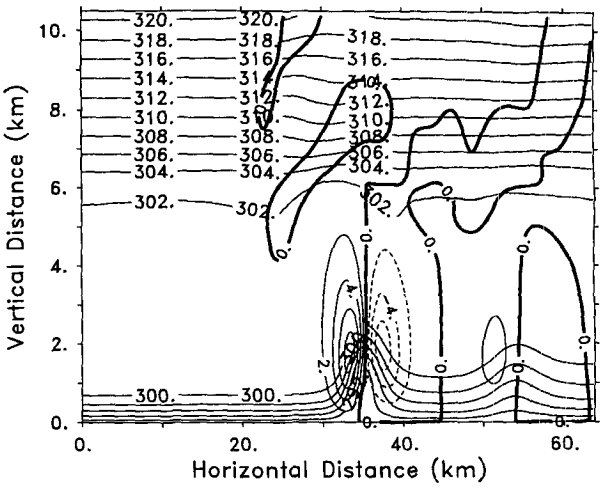


FIG. 11. Results from experiment 4 of potential temperature and vertical motion with Ri = 0.0 and $U_{min} = -10$. Contour intervals are the same as Fig. 3a.

More evidence indicating a possible role for critical levels in squall line development is found in the modeling work of Weisman et al. (1988). As shown in their sensitivity analysis, moderately strong low-level shear in the same direction as the outflow motion is essential for strong squall line development. Weisman et al. have identified a vertically opposing nonhydrostatic pressure gradient in weak low-level shear cases that may prevent strong squall line development. Simulations with the bore initial condition used in this paper yield a similar pressure field; however, the nonhydrostatic pressure gradient is only marginally less with weak shear cases. An alternative explanation for the importance of shear could be critical level interaction with the surface outflow. With gravity wave reflection, the outflow-generated updraft could provide more upward motion and stronger convective redevelopment, but only when sufficient shear exists. In cases with weak low-level shear, a critical level would not be active and the outflow would decay more rapidly than in the trapped case.

Atmospheric conditions similar to those used in experiments 3 and 4 have been observed with many early morning wave systems. A summary of ambient conditions during solitary wave events is given by Crook (1988) demonstrating a consistent pattern of vertical shear with cnoidal wave events. In nearly all of the cases reported, the low-level wind opposes the wave propagation while the winds aloft are either light or in the same direction as the wave propagation. Furthermore, Uccellini and Koch (1987) present evidence supporting a significant role for overreflection with solitary and cnoidal waves of depression. Of the cases discussed by Uccellini and Koch, 10 out of 13 were reported to have a critical level. In the few cases where Ri was reported, Ri was less than 0.25 and a critical level was detected.

In summary, the effects of critical levels are shown to vary significantly depending on the vertical temperature structure of the atmosphere. If stratification is strong below and at the critical level, cnoidal wave systems are absorbed by the mean flow. As the stratification is decreased, absorption is gradually replaced with wave reflection. Once the hydrodynamic stability reaches a Ri threshold of about 0.25, the cnoidal wave system reflects almost entirely with enhanced cnoidal wave growth occurring when Ri is less than 0.25. The exponential decay of gravity wave systems as they approach the critical level prevents absorption from occurring. Therefore, as stability is decreased, only long wavelength features can still be absorbed as they propagate toward the critical level. As shown by the simulations, the requirement for an upper-level propagation layer, as suggested in a linear analysis by Lindzen and Barker (1985), is not essential for cnoidal wave amplification. In fact, the upper-level propagation layer leads to less cnoidal wave growth because of increased transmitted wave energy.

The results from this paper indicate that critical levels can have significant impacts on gravity wave stability. In nearly all cnoidal wave cases, the critical level produced a different wave response than the noncritical layer situation. With other atmospheric disturbances, such as mesoscale waves of depression or squall lines, it is likely that critical levels also play an important instability role. Of particular need is a morphological study of waves of depression. Solitary waves of depression are of importance because of the variety of weather they produce, such as significant snow squalls and strong surface wind gusts. Unlike the undular bore simulations presented here, it is not clear how waves of depression are generated. Defining the initial conditions that lead to solitary waves of depression is therefore not a trivial task. Other factors that should be examined include the effects of moist processes, particularly when a stable atmosphere becomes conditionally unstable. As shown in this paper, neutral conditions generally lead to the most unstable critical level effects.

*Acknowledgments.* Much of this work was performed at the University of Wisconsin as part of my Ph.D. dissertation. I am grateful to Dr. Verner E. Suomi for providing support and advice while I was at school. I would also like to thank Chris Doran, Dave Bader, and Van Ramsdell for providing very useful comments and suggestions on this research and Donald Denbo for the use of his graphics package, PPLUS. This work was partially supported by the U.S. Department of Energy under Contract DE-AC06-76RL0 1830. Pacific Northwest Laboratory is operated by Battelle Memorial Institute for the U.S. Department of Energy.

## REFERENCES

Anderson, J. R., K. K. Droegemeier and R. B. Wilhelmson, 1985: Simulation of the thunderstorm subcloud environment. Preprints, *14th Conf. on Severe Local Storms,* Indianapolis, Amer. Meteor. Soc., 147–150.

Benjamin, T. B., 1967: Internal waves of permanent form in fluids of great depth. *J. Fluid Mech.,* **29,** 559–592.

Booker, J. R., and F. P. Bretherton, 1967: The critical layer for internal gravity waves in shear flow. *J. Fluid. Mech.,* **27,** 513–539.

Bosart, L. F., and F. Sanders, 1986: Mesoscale structure in the Megalopolitan Snowstorm of 11–12 February 1983. Part III: A large-amplitude gravity wave. *J. Atmos. Sci.,* **43,** 924–939.

Bretherton, F. P., 1966: The propagation of groups of internal gravity waves in a shear flow. *Quart. J. Roy. Meteor. Soc.,* **92,** 466–480.

Chimonas, G., and C. O. Hines, 1986: Doppler ducting of atmospheric gravity waves. *J. Geophys. Res.,* **91,** 1219–1230.

Christie, D. R., 1989: Long nonlinear waves in the lower atmosphere. *J. Atmos. Sci.,* **46,** 1462–1491.

——, K. J. Muirhead and A. L. Hales, 1978: On solitary waves in the atmosphere. *J. Atmos. Sci.,* **35,** 805–825.

Cotton, W. R., and G. T. Tripoli, 1978: Cumulus convection in shear flow three-dimensional numerical experiments. *J. Atmos. Sci.,* **35,** 1503–1521.

——, M.-S. Lin, R. L. McAnelly and C. J. Tremback, 1989: A composite model of mesoscale convective complexes. *Mon. Wea. Rev.,* **117,** 765–783.

Crook, N. A., 1986: The effect of ambient stratification and moisture on the motion of atmospheric undular bores. *J. Atmos. Sci.,* **43,** 171–181.

——, 1988: Trapping of low-level internal gravity waves. *J. Atmos. Sci.,* **45,** 1533–1541.

Doviak, R. J., and R. Ge, 1984: An atmospheric solitary gust observed with a doppler radar, a tall tower and a surface network. *J. Atmos. Sci.,* **41,** 2559–2573.

Durran, D. R., and J. B. Klemp, 1983: A compressible model of the simulation of moist mountain waves. *Mon. Wea. Rev.,* **111,** 2341–2361.

Eliassen, A., and E. Palm, 1960: On the transfer of energy in stationary mountain waves. *Geofys. Publ.,* **22,** 1–23.

Grimshaw, R., 1981: A second-order theory for solitary waves in deep fluids. *Phys. Fluids,* **24,** 1611–1618.

Haase, S. P., and R. K. Smith, 1984: Morning glory wave clouds in Oklahoma: A case study. *Mon. Wea. Rev.,* **112,** 2078–2089.

Jones, W. L., 1968: Reflexion and stability of waves in stably stratified fluids with shear flow. *J. Fluid Mech.,* **34,** 609–624.

Klemp, J. B., and R. B. Wilhelmson, 1978: The simulation of three-dimensional convective storm dynamics. *J. Atmos. Sci.,* **35,** 1070–1096.

——, and D. R. Durran, 1983: An upper boundary condition permitting internal gravity wave radiation in numerical mesoscale models. *Mon. Wea. Rev.,* **111,** 430–445.

Lin, Y.-L., and R. C. Goff, 1988: A study of a mesoscale solitary wave in the atmosphere originating near a region of deep convection. *J. Atmos. Sci.,* **45,** 194–205.

Lindzen, R. S., and K. K. Tung, 1978: Wave overreflection and shear instability. *J. Atmos. Sci.*, **35,** 1626–1632.

——, B. Farrell and K. Tung, 1980: The concept of wave overreflection and its application to baroclinic instability. *J. Atmos. Sci.*, **37,** 44–63.

——, and J. W. Barker, 1985: Instability and wave over-reflection in stably stratified shear flow. *J. Fluid Mech.*, **151,** 189–217.

Orlanski, I., 1976: A simple boundary condition for unbounded hyperbolic flows. *J. Comput. Phys.*, **21,** 251–269.

Pecnick, M. J., and J. A. Young, 1984: Mechanics of a strong subsynoptic gravity wave deduced from satellite and surface observations. *J. Atmos. Sci.*, **41,** 1850–1862.

Purdom, J. F. W., 1976: Some uses of high resolution GOES imagery in the mesoscale forecasting of convection and its behavior. *Mon. Wea. Rev.*, **104,** 1474–1483.

Skyllingstad, E. D., 1986: The effects of stratification and vertical wind shear on atmospheric solitary and cnoidal gravity waves: A numerical investigation. Ph.D. thesis, University of Wisconsin-Madison, 161 pp.

Schlesinger, R. E., 1990: Feedback of deep moist convection to its near environment as diagnosed from three-dimensional numerical model output: Results from an early experiment. *J. Atmos. Sci.*, **47,** 1390–1412.

Scorer, R. S., 1949: Theory of lee wave of mountains. *Quart. J. Roy. Meteor. Soc.*, **75,** 41–56.

Smolarkiewicz, P. K., 1983: A simple positive definite advection scheme with small implicit diffusion. *Mon. Wea. Rev.*, **111,** 479–486.

Uccellini, L. W., and S. E. Koch, 1987: The synoptic setting and possible energy sources for mesoscale wave disturbances. *Mon. Wea. Rev.*, **115,** 721–729.

Weisman, M. L., J. B. Klemp and R. Rotunno, 1988: Structure and evolution of numerically simulated squall lines. *J. Atmos. Sci.*, **45,** 1990–2012.